HHS Public Access

Author manuscript

Neurobiol Dis. Author manuscript; available in PMC 2023 January 10.

Published in final edited form as:

Neurobiol Dis. 2022 December ; 175: 105923. doi:10.1016/j.nbd.2022.105923.

Neonatal ketamine exposure impairs infrapyramidal bundle pruning and causes lasting increase in excitatory synaptic transmission in hippocampal CA3 neurons

Omar Hoseá Cabrera[a,1], **Nemanja Useinovic**[a,1], **Stefan Maksimovic**[a], **Michelle Near**[a], **Nidia Quillinan**[a,c], **Slobodan M. Todorovic**[a,c], **Vesna Jevtovic-Todorovic**[a,b,*]

[a]University of Colorado School of Medicine at Anschutz Medical Campus, Department of Anesthesiology, Aurora, CO, USA

[b]University of Colorado School of Medicine at Anschutz Medical Campus, Department of Pharmacology, Aurora, CO, USA

[c]University of Colorado School of Medicine at Anschutz Medical Campus, Neuroscience Graduate Program, Aurora, CO, USA

Abstract

Preclinical models demonstrate that nearly all anesthetics cause widespread neuroapoptosis in the developing brains of infant rodents and non-human primates. Anesthesia-induced developmental apoptosis is succeeded by prolonged neuropathology in the surviving neurons and lasting cognitive impairments, suggesting that anesthetics interfere with the normal developmental trajectory of the brain. However, little is known about effects of anesthetics on stereotyped axonal pruning, an important developmental algorithm that sculpts neural circuits for proper function. Here, we proposed that neonatal ketamine exposure may interfere with stereotyped axonal pruning of the infrapyramidal bundle (IPB) of the hippocampal mossy fiber system and that impaired pruning may be associated with alterations in the synaptic transmission of CA3 neurons. To test this hypothesis, we injected postnatal day 7 (PND7) mouse pups with ketamine or vehicle over 6 h and then studied them at different developmental stages corresponding to IPB pruning (PND20-40). Immunohistochemistry with synaptoporin (a marker of mossy fibers) revealed that in juvenile mice treated with ketamine at PND7, but not in vehicle-treated controls, positive IPB fibers extended farther into the stratum pyramidale of CA3 region. Furthermore, immunofluorescent double labeling for synaptoporin and PSD-95 strongly suggested that the

*Corresponding author. vesna.jevtovic-todorovic@cuanschutz.edu (V. Jevtovic-Todorovic).

[1]Authors have contributed equally to the manuscript.

Author contributions

OHC, SMT, VJT, NQ and NU planned experiments and wrote the manuscript; OHC performed ex vivo electrophysiological experiments and analyzed data; NU performed immunohistological experiments and analyzed the data. SM and MN performed immunohistological experiments. All authors reviewed the manuscript.

All authors contributed to this work according to the International Committee of Medical Journal Editors guidelines.

Declaration of Competing Interest

The authors declare that the research was conducted in the absence of any commercial or financial relationships that could be construed as a potential conflict of interest.

Appendix A. Supplementary data

Supplementary data to this article can be found online at https://doi.org/10.1016/j.nbd.2022.105923.

unpruned IPB caused by neonatal ketamine exposure makes functional synapses. Importantly, patch-clamp electrophysiology for miniature excitatory postsynaptic currents (mEPSCs) in acute brain slices ex vivo revealed increased frequency and amplitudes of mEPSCs in hippocampal CA3 neurons in ketamine-treated groups when compared to vehicle controls. We conclude that neonatal ketamine exposure interferes with normal neural circuit development and that this interference leads to lasting increase in excitatory synaptic transmission in hippocampus.

Keywords

Glutamate; hippocampus; Neonate; Neurotoxicity; Neurotransmission

1. Introduction

In modern neonatal medicine, use of anesthetics is necessary to perform life-saving interventions with minimal discomfort or for prolonged sedation of children in intensive care units. However, preclinical models demonstrate that nearly all anesthetics – as well as sedative and anti-epileptic agents – cause widespread neurotoxicity in infant rodents and non-human primates (Bittigau et al., 2002; Jevtovic-Todorovic et al., 2003; Creeley et al., 2014). Anesthesia-induced developmental neurotoxicity leads to the apoptotic loss of millions of neurons in brain regions that participate in higher order cognition. Indeed, animals anesthetized as neonates have profound impairments in multiple cognitive domains lasting into adulthood (Jevtovic-Todorovic et al., 2003; Paule et al., 2011). Alarmingly, over a dozen clinical studies have associated neonatal anesthesia in human infants with cognitive deficits in later life (Wilder et al., 2009; Flick et al., 2011; Ing et al., 2012, 2021; Lin et al., 2017), and the US Food and Drug Administration recently warned clinicians to discuss with parents the neurocognitive risks of anesthesia to the infant brain (U.S. Food and Drug Administration, 2016, 2018).

The developing brain is most vulnerable to the neurotoxic effects of anesthetics during synaptogenesis, a period of exuberant synapse formation, with presynaptic axons synapsing with more postsynaptic targets than necessary (Tau and Peterson, 2010). Synaptogenesis is followed by protracted refinement of neural circuitry at the microscopic and macroscopic levels, which eliminates functionally inappropriate or quiescent connections between neurons (Kantor and Kolodkin, 2003; Riccomagno and Kolodkin, 2015). A canonical example of macroscopic neural circuit refinement is stereotyped axonal pruning in which axon tracts transiently innervate populations of neurons before being dismantled as development proceeds (O'Leary and Stanfield, 1986). This developmentally regulated pruning algorithm is critical for normal brain development and occurs in many neural circuits, including the infrapyramidal bundle (IPB) of the hippocampus (Cheng et al., 2001; Bagri et al., 2003; Liu et al., 2005). However, possible effects of an early anesthesia exposure on the axonal pruning in developing brain is not well studied.

The hippocampus is comprised of sequential neural circuits that process information in a primarily feed-forward manner from dentate gyrus (DG) to CA3 to CA1 to subiculum. Granule cell axons of the DG give rise to the main bundle (MB) of the mossy fibers

system, which projects to the CA3 region of the hippocampus. The mossy fibers of the MB *permanently* innervate the apical dendrites of CA3 neurons, while those of the IPB *transiently* innervate basal dendrites of nearly all CA3 neurons (Fig. 1A). In early neonatal life, the IPB traverses the length of CA3, releasing the excitatory neurotransmitter glutamate onto large basal dendritic spines (Bagri et al., 2003; Liu et al., 2005). As development proceeds, however, IPB fibers that are distal to DG are pruned beginning in early adolescence – approximately at PND20 in rodents (Bagri et al., 2003) – leaving only proximal branches and synapses by late adolescence (PND40; Fig. 1B).

Recently, we reported that neonatal anesthesia interferes with IPB pruning (Obradovic et al., 2018). We found that mice anesthetized for 6 h with ketamine, a surgical anesthetic of the glutamate *N*-methyl-D-aspartate (NMDA) receptor antagonist class, on PND7 had abnormally long IPB length throughout adolescence. However, the functional consequences of ketamine impairment of IPB pruning on the DG-CA3 neural circuit are unclear.

We hypothesized that neonatal ketamine administration interferes with normal neural circuit development in hippocampus by impairing IPB pruning. We further hypothesized that impaired pruning would manifest functionally as increased synaptic transmission in CA3 neurons still receiving glutamatergic input from the unpruned IPB. We evaluated IPB length and/or excitatory synaptic transmission at three developmental stages coinciding with the window of IPB pruning (Fig. 1C): beginning of pruning (PND20), active pruning (PND30), and end of pruning (PND40). We report that neonatal ketamine exposure impaired IPB pruning and increased spontaneous excitatory synaptic transmission in CA3 neurons.

2. Materials and methods

2.1. Animals

We used litters of CD1 mouse pups of both sexes bred in-house and maintained on a 14/10 light-dark cycle. All procedures were approved by, and in accordance with, the University of Colorado Anschutz Medical Campus Institutional Animal Care and Use Committee protocols.

2.2. Neonatal ketamine administration

Ketamine is one of the few general anesthetics that is clinically used in pediatric intensive care unit for prolonged sedation. Hence, we used an animal model where PND7 CD1 mouse pups were injected intraperitoneally (IP) with a sedative dose of ketamine (Hospira, USA) at 40 mg/kg, or an equal volume of vehicle every 90 min for a total of four injections over 6 h. All mice injected with ketamine lost righting reflex, but generally responded to painful stimuli (tail and toe pinch). Pups were maintained at 35 °C in temperature-controlled anesthesia chambers (Harvard Apparatus, USA). After the 6 h experimental period, pups were monitored until they recovered righting reflex and mobility, then they were returned to their home cage. They were weaned on PND20 and used for morphometric and electrophysiological studies on PND20, PND30, or PND40.

2.3. Synaptic electrophysiology

2.3.1. Region of interest—Miniature excitatory postsynaptic currents (mEPSCs) were recorded from acute hippocampal slices derived from PND20, PND30 or PND40 mice. Using preliminary morphometric data, we computed that by PND30 in control animals, the IPB was pruned to approximately 60% the length of CA3 as measured from the tip of the inferior blade of the DG. Thus, we recorded from pyramidal CA3 neurons that were approximately at 60% the length of CA3. Recording location was further confirmed by neurobiotin histology (data not shown). This process was aided by the fact that CA3 pyramidal neurons have a unique morphology and larger diameter than other cell types in CA3 (Cutsuridis et al., 2010). Our strategy ensured that we recorded from pyramidal neurons that were likely still receiving glutamatergic input from the IPB.

2.3.2. Preparation—To preserve CA3 neuron integrity, we used sucrose-based perfusion, cutting, and incubation solution with reduced sodium and calcium and increased magnesium concentrations in modified from previous slice electrophysiology studies on the mossy fiber system (Bischofberger et al., 2006b) in which horizonal slices are derived from trimming the dorsal part of the brain before glued to the stage. We trimmed the ventral part of the brain to achieve a similar effect to preserve the mossy fibers. Furthermore, consistent with Bischofberger et al. (2006b), we used a vibratome (Leica VT 1200S; Leica Biosystems, USA) with minimal vertical vibrations to obtain hippocampal slices in reduced sodium and calcium and increased magnesium cutting solutions. The sucrose-based solution was comprised of the following (in mM): NaCl 87, KCl 2.5, $CaCl_2$ 0.5, NaH_2PO_4 1.25, $NaHCO_3$ 25, D-glucose 25, Sucrose 75, and $MgCl_2$ 7. Osmolarity was restricted to ~320 mOSm and pH adjusted to ~7.4.

At the determined experimental endpoint, mice were briefly anesthetized with isoflurane and transcardially perfused with cold sucrose-based solution. Brains were rapidly extracted on ice and chilled in carbogenated cold sucrose-based solution before being mounted on a pre-chilled stage and submerged in cold sucrose-based solution for sectioning. Acute hippocampal slices (300 μm thickness) were obtained in the horizontal orientation to ensure the integrity of mossy fiber axons. Slices were transferred immediately to an incubation chamber of carbogenated, warm sucrose-based solution. Slices were allowed to recover for 30 min at 35 °C followed by 15 min at room temperature. Our methodology allowed for healthy slices and stable recordings from pyramidal neurons in the CA3 region of hippocampus over the course of many hours.

2.3.3. Recordings—For mEPSC recordings, slices were transferred to a recording chamber and continuously perfused with carbogenated, low calcium artificial cerebrospinal fluid (ACSF) external solution for at least 10 min to flush any residual sucrose-based solution from the slices. Low calcium ACSF external solution consisted of the following (in mM): NaCl 125, KCl 2.5, $CaCl_2$ 0.5, NaH_2PO_4 1.25, $NaHCO_3$ 24, D-glucose 11, and $MgCl_2$ 1. Osmolarity was 300–310 mOsm and pH was ~7.4.

We recorded mEPSCs with internal solution which consisted of the following (in mM): K-gluconate 135, NaCl 8, MgCl2 1, HEPES 10, EGTA 0.1, MgATP 4, and Na2GTP 0.3.

Osmolarity was between 270 and 280 mOsm, and pH was ~7.3. Neurobiotin (1%) was included in the internal solution to confirm the identity of the neuron.

In the patch-clamp configuration, CA3 neurons were held at −70 mV and mEPSCs were isolated in the presence of 250 nM tetrodotoxin to block voltage-gated sodium currents and 100 μM picrotoxin to block $GABA_A$ inhibitory currents. When a gigaohm seal was established, the cell was accessed and allowed to equilibrate for at least three minutes before recordings. Membrane capacitance, series resistance, and tau (change in membrane potential over time) were monitored continuously.

2.3.4. Inclusion criteria—Recordings in which the series resistance changed by >20% were excluded from analysis. The threshold for inclusion in the dataset was a neuron with at least 100 mEPSCs recorded over a three-minute epoch. Limits for mEPSCs were set at 2.5 times the root mean square of baseline noise and filtered via custom scripts written in MATLAB (MathWorks, USA). We analyzed mEPSCs with pClamp 10 software (Molecular Devices, USA) for frequency (Hz), amplitude (picoamps, pA), rise time (ms), and decay (ms).

2.4. Immunohistochemistry and Immunofluorescence

Previously, we have shown impairment of IPB pruning following neonatal ketamine by using calbindin immunohistochemistry to visualize the mossy fibers (Obradovic et al., 2018). Here, we used synaptoporin (also known as synaptophysin-2), a presynaptic marker which was reported to more selectively labels hippocampal mossy fibers (Singec et al., 2002).

At the determined experimental endpoint, animals dedicated to histology were deeply anesthetized with isoflurane and transcardially perfused with ice-cold phosphate buffered saline (PBS) followed by 4% PFA. Brains were post-fixed in 4% PFA overnight at 4 °C, extracted the following day and embedded in 3% agarose for immediate sectioning in coronal orientation at 50 μm thickness (Leica VT 1200S vibrotome; Leica Biosystems, USA).

For immunofluorescence studies, free floating sections (one per well) were washed three times in PBS plus 0.3% Triton X-100 to permeabilize the membranes. Slices were blocked for 15 min in Background Sniper™ blocking solution (SKU:BS966; Biocare Medical, USA). Slices were then briefly rinsed in PBS plus 0.3% Triton X-100 and incubated overnight at 4 °C with following antibodies: 1:250 guinea pig anti-mouse PSD-95 (124,014; Synaptic Systems, Germany), 1:500 rabbit anti-mouse synaptoporin (102,002; Synaptic Systems, Germany), and 1:500 mouse anti-mouse calbindin (sc-365,360; Santa Cruz Biotechnology, USA). The following day, slices were washed three times with PBS plus 0.3% Triton X-100, then incubated with the following secondary antibodies: 488 donkey anti-guinea pig (706-545-148; Jackson ImmunoResearch, USA) at 1:500, 594 donkey anti-rabbit (711-585-152; Jackson ImmunoResearch, USA) at 1:500, and 647 donkey anti-mouse (715-605-150; Jackson ImmunoResearch, USA) at 1:500 to visualize PSD-95, synaptoporin and calbindin, respectively. Brain slices were mounted onto Superfrost Plus microscopy slides (12-550-15; Fisher Scientific, USA), coverslipped with VECTASHIELD Vibrance

Antifade Mounting Medium (H-1700; Vector, USA) and kept at 4 °C until imaging. In control experiments omitting single or multiple of the primary antibodies, no specific staining was observed in their respective fluorescent channels.

2.5. Confocal imaging

Confocal images were obtained by a blinded observer at 10× or 60× on an Olympus FV-1200 confocal laser scanning microscope (Olympus Corporation, Japan). For IPB length quantification and synaptoporin/calbindin colocalization assessment, high resolution images (2048 × 2048) were obtained at 10× as a 12–14 μm stack, with 2 μm step size. For qualitative histological assessment of synapses, high resolution (2048 × 2048) 60× images were obtained under immersion oil as a 4–5 μm stack, with 0.5 μm step size.

2.6. Analysis of IPB pruning

To account for differences in brain size, IPB pruning was quantified by normalizing IPB length to the length of CA3 (Fig. 1). To obtain consistent measurements of the IPB, synaptoporin-stained coronal sections corresponding to −2.18 mm from bregma in The Mouse Brain in Stereotaxic Coordinates (Franklin and Paxinos, 2008) were used for analysis. At this level, the IPB emerges from the tip of the inferior blade of DG and traverses CA3 through stratum oriens. Images were thresholded and size-filter was applied for particles <0.5 μm radius to eliminate background noise. A blinded observer measured the length of CA3 from the tip of the inferior blade of the dentate gyrus to the apex of the CA3 curvature (“a”) (Fig. 2A and B). Then the IPB was measured from the tip of the inferior blade of the dentate gyrus to its most distal portion (“b”). Normalized IPB length was calculated as:

$$\text{Normalized IPB length} = \text{IPB length } (\mu\text{m})/\text{ CA3 length } (\mu\text{m}) < \geq \text{“b ”/“ a”}$$

Values were multiplied by 100 to express normalized IPB length as a percent length of CA3.

To gain further insight into the IPB pruning, we performed analysis of percent area of stain of synaptoporin-labeled IPB *en route* through stratum oriens (Fig. 3C). The analysis was done on thresholded binary images in three predetermined regions, each corresponding to one-third of the CA3 length (“a” / 3), and labeled as “proximal”, “mid”, and “distal” rectangular area, with regard to their proximity to the hilus of DG. The long axis of the rectangle corresponded to one-third of the CA3 length in μm (“a” / 3), and the short axis was set at a fixed value of 100 μm. The analysis was performed in FIJI open-source software (Schindelin et al., 2012) and expressed as percent area of stain within the given rectangle.

2.7. Experimental design and statistical analyses

IPB normalized length data were analyzed via two-way ANOVA (Treatment × Age) followed by Sidak’s post-hoc analysis corrected for multiple comparisons. Area of stain analysis was performed via multiple unpaired *t*-tests followed by Holm-Sidak test to correct for multiple comparisons. There were no sex differences at any developmental stage (Supplementary Material, Table S1). Therefore, we collapsed data across sex for analysis and presentation. Power analysis was based on previous studies (Digruccio et al., 2015;

Obradovic et al., 2018) and conducted with G*Power software (Faul et al., 2007). Power analysis suggested a minimum of six animals per group for IPB analysis and 20 neurons per group for electrophysiology studies. Data were analyzed in Prism 9.3 (GraphPad, USA) and JASP (University of Amsterdam, The Netherlands). α was set at 0.05, thus p-values <0.05 were considered statistically significant. Data are expressed as Mean ± SEM. The Kolmogorov-Smirnov test was used to calculate differences between cumulative frequency distributions. Cohen's d effect size (mean difference between groups expressed in standard deviations; 0.20 = small, 0.40 = medium, 0.80 = large) was calculated for all dependent variables.

3. Results

3.1. Synaptoporin and calbindin as markers of mossy fibers

Previously, we have demonstrated impaired IPB pruning following neonatal ketamine administration using calbindin as an IPB marker (Obradovic et al., 2018). Because calbindin is broadly expressed in mouse hippocampus, we used synaptoporin (Singec et al., 2002) to independently confirm our previous findings. Hence, we co-stained IPB with synaptoporin and calbindin.

Regardless of age, we noted strong immunolabeling of IPB mossy fibers of animals following either vehicle (Fig. 2A and C) or ketamine treatment (Figs. 2B and 3D). The majority of synaptoporin immunoreactivity was confined to stratum oriens and stratum lucidum (corresponding to IFB and MB fibers, respectively) (Fig. 2A and B). In addition to regions stained with synaptoporin, calbindin-labeled hippocampal structures exhibited immunoreactivity more broadly, extending further into the stratum radiatum, pyramidale and lacunosum-moleculare, as well as layers of the dentate gyrus (Fig. 2C and D). Mossy fibers of IPB were readily observable on either synaptoporin or calbindin staining. The general appearance of the IPB was a bundle of fibers emanating from the hilus of the DG and running in an anterolateral direction through stratum oriens. Axon collaterals of the IPB curved from stratum oriens to stratum pyramidale where CA3 neurons are located. Because synaptoporin immunoreactivity was more confined, virtually limited to stratum oriens and stratum lucidum, compared to calbindin, we concluded that synaptoporin was more suitable as a marker of mossy fiber system in the mouse hippocampus.

3.2. Neonatal ketamine treatment impaired IPB pruning

Next, we quantified IPB pruning by determining normalized IPB length between groups, which was calculated as the length of the IPB divided by the length of CA3 (Fig. 3A and B). Statistical analysis revealed significant main effect of Treatment ($F = 12.66$, $p < 0.001$) and Age ($F = 16.64$, $p < 0.001$). We did not observe a significant Treatment × Age interaction ($F = 2.08$, $p = 0.13$).

At PND20, when IPB pruning is beginning, post hoc multiple comparisons revealed that there was no difference in normalized IPB length between the vehicle (77.65% ± 2.23; $n = 10$) and ketamine (79.45% ± 3.48; $n = 9$) groups, $p = 0.98$, Cohen's $d = 0.21$ (Fig. 3D). At PND30, when the IPB is being developmentally pruned, the IPB was about 13% shorter in

mice treated with vehicle as neonates (62.56% ± 3.86; $n = 12$) compared to those treated with ketamine (75.73% ± 3.55; $n = 9$), $p = 0.02$, Cohen's $d = 1.09$. At PND40, the IPB remained about 15% longer in ketamine mice (66.11% ± 3.50; $n = 9$) relative to vehicle mice (51.62% ± 3.06; $n = 11$), $p = 0.01$, Cohen's $d = 1.41$.

To further elucidate whether pruning occurs proportionally along the length of the IPB, or more heavily affects certain portions of the IPB, we performed analysis of synaptoporin-stained area in three rectangular zones of stratum oriens traversed by the IPB, labeled with regard to their proximity to DG (Fig. 3C). The percent area of stain was then compared between ketamine and vehicle treatments for each of the timepoints – at PND20, PND30 and PND40 – for each of the zones separately. In the area most proximal to the DG, we observed no significant differences between treatments across all three timepoints ($p = 0.49$, $p = 0.64$ and $p = 0.59$ for PND20, PND30, and PND40, respectively) (Fig. 3E). Similarly, the percent area of stain in the middle portion did not differ between treatments at any of the timepoints examined ($p = 0.40$, $p = 0.70$ and $p = 0.55$ for PND20, PND30 and PND40, respectively).

In the area most distal to the DG, no difference was noted between ketamine and vehicle groups when examined at PND20 ($p = 0.87$). Although percent area at PND30 were trending towards higher values in ketamine treatment compared to controls, this was not statistically significant ($p = 0.08$). However, when quantified at PND40, the percent area of stain was about 2-fold higher in the ketamine group (0.34% ± 0.05) compared with vehicle (0.15% ± 0.04), $p = 0.03$, Cohen's $d = 1.28$.

Taken together, these data indicate that neonatal ketamine exposure impaired the normal developmental pruning of the IPB, and that this alteration is primarily affecting the most distal portions of the IPB relative to DG.

3.3. Ketamine-induced impairment in IPB pruning and functional synapses

Our qualitative evaluation revealed that in juvenile mice treated with ketamine as neonates, synaptoporin-positive IPB fibers extended into stratum pyramidale, which suggested that the unpruned IPB in ketamine mice was innervating CA3 neurons. We performed immunofluorescent double-labeling at the level of proximal third of IPB to assess if there was evidence of functional synapses made by the IPB in PND40 vehicle and ketamine-treated and vehicle-treated animals (Fig. 4). Sections were double labeled for PSD-95, a postsynaptic scaffolding protein of glutamatergic excitatory neurons, and synaptoporin, a marker of mossy fibers.

As expected, we found that at PND40 in both vehicle and ketamine mice, the IPB sent synaptoporin-positive collaterals from stratum oriens into stratum pyramidale (Fig. 4A and B). The fibers were studded with synaptoporin and PSD-95 positive nodules which were likely large *en passant* boutons characteristic of the mossy fiber system (Liu et al., 2005). Additionally, numerous smaller double-stained puncta were seen surrounding somas and basal dendrites of the pyramidal neurons in either treatment groups. Hence, our qualitative analysis of synaptoporin and PSD-95 positive boutons suggests that the remaining IPB fibers at PND40 make functional synapses. We next used patch-clamp recordings from acute

brain slices at different developmental ages to investigate possible differenes in synaptic transmission between vehicle and ketamine treated cohorts.

3.4. Neonatal ketamine treatment increased excitatory synaptic transmission in CA3 neurons at the start of IPB pruning

Previous studies have demonstrated that spontaneous neurotransmitter release is important for normal synapse development and maturation (Kavalali, 2014). Hence, we assessed spontaneous excitatory synaptic transmission by recording mEPSCs in pyramidal CA3 neurons. Fig. 5A displays representative traces from PND20 juvenile mice treated with vehicle ($n = 8$ mice, $n = 22$ neurons; **left panel**) or with ketamine ($n = 9$ mice, $n = 19$ neurons; **right panel**) as neonates. At PND20, there was increased average frequency of mEPSCs in ketamine mice (8.70 Hz ± 0.95) versus vehicle mice (5.30 Hz ± 0.75), $p = 0.009$, Cohen's $d = 0.87$ (Fig. 5B **left panel**). When we plotted the cumulative frequency of the interevent interval, neonatal ketamine caused a leftward shift, indicating a higher frequency of mEPSC events, $p < 0.0001$ by Kolmogorov-Smirnov test (Fig. 5B **right panel**).

There was no difference in the average amplitude of mEPSCs between the ketamine (−21.08 pA ± 1.42) and vehicle (−19.11 pA ± 0.87) groups, $p = 0.25$, Cohen's $d = 0.36$ (Fig. 5C **left panel**) but a significant rightward shift in the cumulative frequency distribution of mEPSC amplitudes in ketamine-treated mice, $p < 0.001$ by Kolmogorov-Smirnov test (Fig. 5C **right panel**). However, there was also a slight decrease in rise time in ketamine mice (3.80 ms ± 0.20) versus vehicle mice (4.24 ms ± 0.10), $p = 0.04$, Cohen's $d = 0.65$ (Fig. 5D). There was no difference in decay between the ketamine (8.91 ms ± 0.51) and vehicle (8.01 ms ± 0.45) groups, $p = 0.20$, Cohen's $d = 0.41$ (Fig. 5E). Taken together, our data shows that neonatal ketamine exposure caused increased frequency and amplitudes in synaptic transmission of CA3 neurons and a moderate shift towards faster excitatory events.

3.5. Neonatal ketamine treatment increased excitatory synaptic transmission of CA3 neurons at later developmental stages

To study synaptic transmission at later developmental age, we combined PND30 and PND40 cohorts to minimize the number of animals used for mEPSC recordings. Fig. 6A displays representative traces from vehicle ($n = 11$ mice, $n = 30$ neurons; **left panel**) and ketamine ($n = 12$ mice, $n = 22$ neurons; **right panel**) mice. There was increased average frequency of mEPSCs in mice treated with ketamine as neonates (8.86 Hz ± 0.65) compared to those treated with vehicle (6.42 Hz ± 0.67), $p = 0.01$, Cohen's $d = 0.72$ (Fig. 6B **left panel**). At PND30 + PND40, neonatal ketamine treatment caused a leftward shift in cumulative frequency of the interevent interval of all events, also indicating a higher frequency of mEPSC events, $p < 0.001$ by Kolmogorov-Smirnov test (Fig. 6B **right panel**).

There was also a moderate increase in the average amplitude of mEPSCs in ketamine-treated mice (−23.87 pA ± 2.14) compared to vehicle mice (−18.86 pA ± 0.86), $p = 0.04$, Cohen's $d = 0.64$ (Fig. 6C **left panel**) and a significant rightward shift in the cumulative frequency distribution of mEPSC amplitudes, $p < 0.001$ by Kolmogorov-Smirnov test (Fig. 6C **right panel**). In contrast, there was no difference in rise time kinetics in ketamine mice (3.97 ms ± 0.19) versus vehicle mice (4.16 ms ± 0.14), $p = 0.41$, Cohen's $d = 0.23$ (Fig. 6D). Similarly,

there was no difference in decay kinetics in ketamine (7.35 ms ± 0.38) versus vehicle (7.65 ms ± 0.29), $p = 0.52$, Cohen's $d = 0.18$ (Fig. 6E). We conclude that neonatal ketamine treatment significantly increased both frequency and amplitudes of mEPSCs in pyramidal CA3 neurons.

Finally, to quantify the functional mossy fiber-CA3 synapses, we analyzed the high amplitude mEPSCs (>45 pA) in PND30 + 40 ketamine and vehicle-treated mice (Henze et al., 1997). Events with the amplitudes >45 pA were counted and expressed as percentage of total number of recorded events. We observed a significant, 2.5-fold increase in percent of high amplitude mEPSCs in ketamine-treated mice (6.34% ± 1.76) compared to vehicle mice (2.51 ± 0.65), $p = 0.03$, Cohen's $d = 0.65$ (Supplementary Material, Fig. S1). Based on these results, we conclude that neonatal ketamine administration resulted in more functional mossy fiber-CA3 synapses compared to age-matched, vehicle-treated controls.

4. Discussion

The key takeaways from the current study are that neonatal ketamine treatment causes impaired stereotyped axonal pruning of the IPB and increased excitatory synaptic transmission of CA3 neurons in juvenile hippocampus. Notably, these neuropathological alterations occurred and persisted weeks after the initial anesthetic insult, suggesting that anesthetics during infancy can cause long-term dysregulation of neural circuit formation and function.

4.1. Neonatal ketamine impairs IPB pruning

Stereotyped IPB pruning was impeded by neonatal ketamine treatment. Stereotyped axonal pruning is a developmental algorithm that sculpts neural circuits following the exuberant synapse formation that occurs during synaptogenesis (Bagri et al., 2003; Kantor and Kolodkin, 2003). The IPB undergoes substantial stereotyped axonal pruning in the juvenile period in rodents, retracting hundreds of microns towards its source neurons in DG (Bagri et al., 2003). At all juvenile developmental stages, we documented complex variations in IPB morphology, but, in general, the IPB collateralized extensively into CA3 stratum pyramidale *en route* through stratum oriens. As normal development progressed, collaterals distal to DG were lost, leaving only proximal collaterals that innervated CA3. In mice treated with ketamine, however, the IPB remained abnormally long, projecting significantly farther into the distal portions of CA3 compared with age-matched, anesthesia-naïve controls.

In rodent models of *status epilepticus* and in humans with temporal lobe epilepsy, injury to DG causes the IPB to denervate CA3 neurons (Blumcke et al., 2000; Isgor et al., 2015). CA3 denervation is followed by protracted IPB growth as DG granule cells sprout new axons that make inappropriate, recurrent connections to neighboring cells, which contributes to epileptogenesis (Häussler et al., 2016). Given the increased excitatory synaptic transmission we documented in the current study, we speculate that excessive, age-inappropriate glutamate neurotransmission from the unpruned IPB might contribute to seizure-like activity in hippocampus.

Moreover, the DG-CA3 circuit is remodeled after other neonatal neuronal injuries. Similar to anesthetics used for legitimate medical purposes, ethanol is a potent developmental apoptogen when abused by pregnant mothers (Olney et al., 2002a, 2002b). Interestingly, ethanol possesses both NMDA receptor antagonist (Lovinger et al., 1989; PL et al., 1989) and inhibitory γ-aminobutyric acid (GABA) receptor agonist properties (Harris et al., 1995). Furthermore, previous studies have documented that adult rodents exposed to ethanol in utero also have abnormally long IPB fibers that inappropriately impinge on distal CA3 neurons (West et al., 1981). Thus, it is possible that anesthetics that are GABA modulators or that have dual pharmacology also alter the normal morphology and function of the mossy fiber system by interfering with stereotyped axonal pruning.

4.2. Unpruned IPB forms boutons

Our confocal images suggested that in mice treated with ketamine as neonates, the unpruned IPB formed functional synapses with CA3 neurons. As the unmyelinated axons of the mossy fiber system course through stratum pyramidale, they produce *en passant* boutons arranged as large and elaborate synaptic complexes (Amaral et al., 2007). Ultrastructural studies have shown that in early development, IPB boutons on the basal dendrites of CA3 neurons are comprised of multiple asymmetrical synapses that are positive for vesicular glutamate transporters and for NMDA receptor subunit 1 (Liu et al., 2005), markers of glutamatergic synapses.

When we double labeled IPB for synaptoporin and PSD-95, there was clear evidence of IPB boutons in stratum pyramidale of CA3 at PND40, in both ketamine- and vehicle-treated mice. Within stratum pyramidale, synaptoporin and PSD-95 positive boutons formed clumps. These observations imply that the unpruned IPB likely forms functional synapses with CA3 neurons, which is supported by our electrophysiology data.

4.3. Excitatory synaptic transmission is chronically altered

Because the primary neurotransmitter of the mossy fiber system is glutamate (Crawford and Connor, 1973), we posit that impaired pruning of the IPB caused by neonatal ketamine treatment may be associated with altered function of excitatory synaptic transmission in CA3 neurons. Previous studies have demonstrated that spontaneous neurotransmitter release is particularly important for normal synapse development, maturation, and plasticity (Kavalali, 2014; Andreae and Burrone, 2018). Hence, we chose to focus on a neurotransmission modality that is relevant to normal brain development and that may be altered following neonatal anesthesia. Indeed, in our measures of excitatory synaptic transmission, we found higher frequency and amplitudes, as well as faster kinetics of mEPSCs in ketamine treated group, which strongly suggest that both presynaptic and postsynaptic mechanisms are involved, respectively.

Notably, changes in frequency were apparent in the early juvenile period at the beginning of IPB pruning and persisted throughout the developmental pruning window, consistent with long-term dysregulation of excitatory neurotransmission. Additionally, more prominent increases in the amplitude of mEPSCs that we observed at later developmental stages may indicate more vesicular glutamate and/or enlargement of glutamate vesicles in mice treated

with ketamine as neonates. Our data are consistent with previous studies that reported that the acute effects of ketamine and other NMDA receptor antagonists on synaptic plasticity in the hippocampal CA1 region could be mimicked by selective suppression of spontaneous, action potential independent synaptic release by depleting spontaneously recycling vesicles (Nosyreva et al., 2013). Importantly, it is well documented that mEPSCs are involved in rapid synaptic homeostasis and serve to stabilize synaptic function (Sutton et al., 2006; Huupponen et al., 2007). Furthermore, spontaneous synaptic release is altered in several brain regions following neonatal anesthesia exposure as we demonstrated previously (Digruccio et al., 2015; Dalla Massara et al., 2016; Woodward et al., 2019). Hence, we speculate that effects of ketamine on the amplitude and frequency of mEPSCs that we observed at PND20 may drive synaptic stability and thus less pruning at PND30–40.

Neonatal ketamine treatment also affected parameters of postsynaptic excitatory transmission. As pruning began, we documented shortened rise times of mEPSC events and, in later developmental stages, we noted a 25% increase in mEPSC amplitude. Changes in rise time and amplitude may suggest altered postsynaptic glutamate receptor kinetics or the number or types of receptors activated. For example, the ionotropic alpha-amino-3-hydroxy-5-methyl-4-isoxazolepropionic acid (AMPA) receptor mediates fast excitatory neurotransmission, and AMPA currents tend to have faster kinetics and larger amplitude events than those generated by glutamatergic kainate or NMDA receptors. Following neonatal exposure to a triple anesthetic cocktail of midazolam, isoflurane, and nitrous oxide, DiGruccio and colleagues (2015) documented hyperexcitability of the thalamocortical neural circuit that manifested as an increase in the AMPA component of excitatory currents. A similar alteration in AMPA-mediated neurotransmission may be responsible for our observation of shortened rise times and larger amplitude of excitatory events. Alternatively, faster rise times of mEPSCs in the ketamine-treated group could be due to more dense excitatory synapses further away from the soma, or a change in the maturation of CA3 pyramidal cells, as well as indirect effects due to increased branching of CA3 neurons.

There are some limitations to the current study. Given that CA3 neurons receive massive excitatory input from the mossy fibers which synapse on the proximal (to soma) areas of the apical and basal dendritic trees, these strong synapses provide fast excitatory synaptic transmission in CA3 because of their size and large pool of glutamatergic vesicles (Bischofberger et al., 2006a). However, neuronal excitation in CA3 is driven by multiple synaptic inputs, including from local CA3 granule cells (Szabadics et al., 2010), recurrent CA3-CA3 synapses, and perforant path fibers (Yeckel and Berger, 1990). Importantly, mEPSCs with the amplitudes >45 pA were in previous study specifically linked to mossy fibers-CA3 synapse (Henze et al., 1997) and we found that these events were increased in ketamine mice when compared to vehicle group. While it is reasonable to infer that the mEPSCs recorded in this study originated mainly from mossy fiber axons of the MB and of the IPB, the precise presynaptic contributions to the excitatory input of pyramidal CA3 neurons in our preparation is not known. Thus, understanding how neonatal ketamine anesthesia affects these contributions could be an important area of future investigation.

4.4. Future outlook

Dysregulation of pre- and postsynaptic neurotransmission mechanisms caused by neonatal ketamine exposure is expected to degrade the computational efficacy of DG-CA3 neural circuitry. The hippocampus is comprised of sequential neural circuits that process information in a primarily feed-forward manner from DG to CA3 to CA1 to subiculum, and we have now documented substantial neuronal plasticity and transmission impairments in each of these circuits. For example, prolonged neonatal exposure to the triple anesthetic cocktail or to ketamine impaired long-term potentiation – the cellular mechanism of learning and memory – in CA1 and subiculum (Jevtovic-Todorovic et al., 2003; Manzella et al., 2020).

Neurons in thalamus project to corresponding areas of sensory cortex, but some thalamocortical axons collateralize transiently into adjacent areas before they are eliminated in later development (Naegele et al., 1988; Catalano et al., 1996). Given thalamocortical network hyperexcitability following exposure to a triple anesthetic cocktail (Digruccio et al., 2015), impaired pruning of these transient collaterals by neonatal anesthesia may explain, in part, the disruption of excitatory neurotransmission in thalamocortical circuitry. Thus, an important and unanswered question is whether neonatal anesthesia interferes with stereotyped axonal pruning of other neural circuits that contribute to higher-order cognitive function. Future studies may also be expanded to investigations of ketamine-induced plasticity of evoked synaptic responses in the CA3 region of hippocampus, as we have done previously in the thalamus following neonatal exposure to a triple combination of midazolam, isoflurane, and nitrous oxide (Digruccio et al., 2015) and to a double combination of isoflurane and nitrous oxide (Woodward et al., 2019).

5. Conclusions

Anesthesia-induced developmental neurotoxicity causes the apoptotic death of millions of otherwise healthy neurons in the developing brain. However, the neuropathological consequences of neonatal anesthesia are evident even in neurons that survive the insult. Anesthetics can dysregulate the genome and epigenome (Dalla Massara et al., 2016; Chastain-Potts et al., 2020; Cabrera et al., 2021), change neuronal and synaptic morphology (Sanchez et al., 2011; Boscolo et al., 2013), and alter neurotransmission (Digruccio et al., 2015; Joksimovic et al., 2020). Indeed, our functional studies strongly suggest that neonatal exposure to general anesthetics can lead to disruptions of circuit development independent of cell death.

In the current study, neonatal ketamine administration impaired stereotyped developmental pruning of the IPB, an axonal tract of the DG-CA3 neural circuit of hippocampus. We also documented increased excitatory synaptic transmission in CA3 neurons. These neuropathological alterations occurred and persisted for weeks after the initial anesthesia exposure. Taken together, our data indicate that anesthetics are potent neurotoxic agents capable of substantially altering the normal developmental trajectory of the mammalian brain.

Supplementary Material

Refer to Web version on PubMed Central for supplementary material.

Funding

This work was supported by the Department of Anesthesiology at the University of Colorado Anschutz Medical Campus, Aurora, CO; Eunice Kennedy Shriver National Institute of Child Health and Human Development, Bethesda, MD [R01HD097990, R01HD044517, R01HD044517-S, R21HD080281; F32HD101357]; National Institute of General Medical Sciences, Bethesda, MD [R01GM118197, R01GM118197-11S1, R35GM141802], March of Dimes National Award, Crystal City, VA; and CU Medicine Endowments, Aurora, CO.

Data availability

Original data from the authors is available upon reasonable request.

References

Amaral DG, Scharfman HE, Lavenex P, 2007. The dentate gyrus: fundamental neuroanatomical organization (dentate gyrus for dummies). Prog. Brain Res. 163.

Andreae LC, Burrone J, 2018. The role of spontaneous neurotransmission in synapse and circuit development. J. Neurosci. Res. 96, 354–359. Available at: https://onlinelibrary.wiley.com/doi/full/10.1002/jnr.24154 [Accessed December 28, 2021]. [PubMed: 29034487]

Bagri A, Cheng HJ, Yaron A, Pleasure SJ, Tessier-Lavigne M, 2003. Stereotyped pruning of long hippocampal axon branches triggered by retraction inducers of the semaphorin family. Cell 113, 285–299. [PubMed: 12732138]

Bischofberger J, Engel D, Frotscher M, Jonas P, 2006a. Timing and efficacy of transmitter release at mossy fiber synapses in the hippocampal network. Pflugers Arch. - Eur. J. Physiol. 453, 361–372. Available at: https://link.springer.com/article/10.1007/s00424-006-0093-2 [Accessed December 28, 2021]. [PubMed: 16802161]

Bischofberger J, Engel D, Li L, Geiger JRP, Jonas P, 2006b. Patch-clamp recording from mossy fiber terminals in hippocampal slices. Nat. Protoc. 1, 2075–2081. [PubMed: 17487197]

Bittigau P, Sifringer M, Genz K, Reith E, Pospischil D, Govindarajalu S, Dzietko M, Pesditschek S, Mai I, Dikranian K, Olney JW, Ikonomidou C, 2002. Antiepileptic drugs and apoptotic neurodegeneration in the developing brain. Proc. Natl. Acad. Sci. 99, 15089–15094. Available at: https://www.pnas.org/content/99/23/15089 [Accessed July 27, 2021]. [PubMed: 12417760]

Blumcke I, Suter B, Behle K, Kuhn R, Schramm J, Elger CE, Wiestler OD, 2000. Loss of hilar mossy cells in ammon's horn sclerosis. Epilepsia 41, S174–S180. [PubMed: 10999540]

Boscolo A, Milanovic D, Starr JA, Sanchez V, Oklopcic A, Moy L, Ori CC, Erisir A, Jevtovic-Todorovic V, 2013. Early exposure to general anesthesia disturbs mitochondrial fission and fusion in the developing rat brain. Anesthesiology 118, 1086–1097. Available at: http://pubs.asahq.org/anesthesiology/article-pdf/118/5/1086/261819/20130500_0-00019.pdf [Accessed March 9, 2021]. [PubMed: 23411726]

Cabrera OH, Useinovic N, Jevtovic-Todorovic V, 2021. Neonatal anesthesia and dysregulation of the epigenome. Biol. Reprod. 30. Available at: https://academic.oup.com/biolreprod/advance-article/doi/10.1093/biolre/ioab136/6320120 [Accessed July 30, 2021].

Catalano SM, Robertson RT, Killackey HP, 1996. Individual axon morphology and thalamocortical topography in developing rat somatosensory cortex. J. Comp. Neurol. 366–402.

Chastain-Potts SE, Tesic V, Tat QL, Cabrera OH, Quillinan N, Jevtovic-Todorovic V, 2020. Sevoflurane exposure results in sex-specific transgenerational upregulation of target IEGs in the subiculum. Mol. Neurobiol. 57.

Cheng HJ, Bagri A, Yaron A, Stein E, Pleasure SJ, Tessier-Lavigne M, 2001. Plexin-A3 mediates semaphorin signaling and regulates the development of hippocampal axonal projections. Neuron 32, 249–263. [PubMed: 11683995]

Crawford IL, Connor JD, 1973. Localization and release of glutamic acid in relation to the hippocampal mossy fibre pathway. Nat 2445416 (244), 442–443. Available at: https://www.nature.com/articles/244442a0 [Accessed July 30, 2021].

Creeley CE, Dikranian KT, Dissen GA, Back SA, Olney JW, Brambrink AM, 2014. Isoflurane-induced apoptosis of neurons and oligodendrocytes in the fetal rhesus macaque brain. Anesthesiology 120, 626–638. Available at: http://insights.ovid.com/crossref?an=00000542-201403000-00022. [PubMed: 24158051]

Cutsuridis V, Graham BP, Cobb S., Vida I (Eds.), 2010. Hippocampal microcircuits. Springer.

Dalla Massara L, Osuru HP, Oklopcic A, Milanovic D, Joksimovic SM, Caputo V, Digruccio MR, Ori C, Wang G, Todorovic SM, Jevtovic-Todorovic V, 2016. General anesthesia causes epigenetic histone modulation of c-Fos and brain-derived neurotrophic factor, target genes important for neuronal development in the immature rat hippocampus. Anesthesiology 124, 1311–1327. [PubMed: 27028464]

Digruccio MR, Joksimovic S, Joksovic PM, Lunardi N, Salajegheh R, Jevtovic-Todorovic V, Beenhakker MP, Goodkin HP, Todorovic SM, 2015. Hyperexcitability of rat thalamocortical networks after exposure to general anesthesia during brain development. J. Neurosci. 35, 1481–1492. Available at: http://www.jneurosci.org/content/35/4/1481.short. [PubMed: 25632125]

Faul F, Erdfelder E, Lang AG, Buchner A, 2007. G*Power 3: a flexible statistical power analysis program for the social, behavioral, and biomedical sciences. Behav. Res. Methods 175–191. [PubMed: 17695343]

Flick RP, Katusic SK, Colligan RC, Wilder RT, Voigt RG, Olson MD, Sprung J, Weaver AL, Schroeder DR, Warner DO, 2011. Cognitive and behavioral outcomes after early exposure to anesthesia and surgery. Pediatrics 128, 273–292.

Franklin KBJ, Paxinos G, 2008. The Mouse Brain in Stereotaxic Coordinates, Compact, 3rd edition. Elsevier, Cambridge, MA. Available at: https://www.elsevier.com/books/the-mouse-brain-in-stereotaxic-coordinates-compact/franklin/978-0-12-374244-5. [Accessed July 30, 2021].

Harris R, Proctor W, McQuilkin S, Klein R, Mascia M, Whatley V, Whiting P, Dunwiddie T, 1995. Ethanol increases GABAA responses in cells stably transfected with receptor subunits. Alcohol. Clin. Exp. Res. 19, 226–232. Available at: https://pubmed.ncbi.nlm.nih.gov/7771653/ [Accessed July 30, 2021]. [PubMed: 7771653]

Häussler U, Rinas K, Kilias A, Egert U, Haas CA, 2016. Mossy fiber sprouting and pyramidal cell dispersion in the hippocampal CA2 region in a mouse model of temporal lobe epilepsy. Hippocampus 26, 577–588. [PubMed: 26482541]

Henze DA, Card JP, Barrionuevo G, Ben-Ari Y, 1997. Large amplitude miniature excitatory postsynaptic currents in hippocampal CA3 pyramidal neurons are of mossy fiber origin. J. Neurophysiol. 77, 1075–1086. [PubMed: 9084583]

Huupponen J, Molchanova SM, Taira T, Lauri SE, 2007. Susceptibility for homeostatic plasticity is down-regulated in parallel with maturation of the rat hippocampal synaptic circuitry. J. Physiol. 581, 505–514. Available at: https://onlinelibrary.wiley.com/doi/full/10.1113/jphysiol.2007.130062 [Accessed March 27, 2022]. [PubMed: 17347263]

Ing C, DiMaggio C, Whitehouse A, Hegarty MK, Brady J, Von Ungern-Sternberg BS, Davidson A, Wood AJJ, Li G, Sun LS, 2012. Long-term differences in language and cognitive function after childhood exposure to anesthesia. Pediatrics 130, e476–e485. [PubMed: 22908104]

Ing C, Landau R, Destephano D, Miles CH, Von Ungern-Sternberg BS, Li G, Whitehouse AJO, 2021. Prenatal exposure to general anesthesia and childhood behavioral deficit. Anesth. Analg 595–605. Available at: https://journals.lww.com/anesthesia-analgesia/Fulltext/2021/09000/Prenatal_Exposure_to_General_Anesthesia_and.8.aspx [Accessed October 3, 2021]. [PubMed: 33497062]

Isgor C, Pare C, McDole B, Coombs P, Guthrie K, 2015. Expansion of the dentate mossy fiber-CA3 projection in the brain-derived neurotrophic factor-enriched mouse hippocampus. Neuroscience 288, 10–23. [PubMed: 25555929]

Jevtovic-Todorovic V, Hartman RE, Izumi Y, Benshoff ND, Dikranian K, Zorumski CF, Olney JW, Wozniak DF, 2003. Early exposure to common anesthetic agents causes widespread neurodegeneration in the developing rat brain and persistent learning deficits. J. Neurosci. 23, 876–882. [PubMed: 12574416]

Joksimovic SM, DiGruccio MR, Boscolo A, Jevtovic-Todorovic V, Todorovic SM, 2020. The role of free oxygen radicals in lasting hyperexcitability of rat subicular neurons after exposure to general anesthesia during brain development. Mol. Neurobiol. 57, 208–216. [PubMed: 31493241]

Kantor DB, Kolodkin AL, 2003. Curbing the excesses of youth: molecular insights into axonal pruning. Neuron 38, 849–852. [PubMed: 12818170]

Kavalali ET, 2014. The mechanisms and functions of spontaneous neurotransmitter release. Nat. Rev. Neurosci. 161 (16), 5–16. Available at: https://www.nature.com/articles/nrn3875 [Accessed December 28, 2021].

Lin EP, Lee JR, Lee CS, Deng M, Loepke AW, 2017. Do anesthetics harm the developing human brain? An integrative analysis of animal and human studies. Neurotoxicol. Teratol. 60, 117–128. Available at: 10.1016/j.ntt.2016.10.008. [PubMed: 27793659]

Liu XB, Low LK, Jones EG, Cheng HJ, 2005. Stereotyped axon pruning via plexin signaling is associated with synaptic complex elimination in the hippocampus. J. Neurosci. 25, 9124–9134. [PubMed: 16207871]

Lovinger DM, White G, Weight F, 1989. Ethanol inhibits NMDA-activated ion current in hippocampal neurons. Science 243, 1721–1724. Available at: https://pubmed.ncbi.nlm.nih.gov/2467382/ [Accessed July 30, 2021]. [PubMed: 2467382]

Manzella FM, Joksimovic SM, Orfila JE, Fine BR, Dietz RM, Sampath D, Fiedler HK, Tesic V, Atluri N, Raol YH, Jevtovic-Todorovic V, Herson PS, Todorovic SM, 2020. Neonatal ketamine alters high-frequency oscillations and synaptic plasticity in the subiculum but does not affect sleep macrostructure in adolescent rats. Front. Syst. Neurosci. 14, 26. Available at: /PMC/articles/PMC7264261/ [Accessed March 9, 2021]. [PubMed: 32528257]

Naegele JR, Jhaveri S, Schneider GE, 1988. Sharpening of topographical projections and maturation of geniculocortical axon arbors in the hamster. J. Comp. Neurol. 277, 593–607. Available at: https://onlinelibrary.wiley.com/doi/full/10.1002/cne.902770411 [Accessed July 30, 2021]. [PubMed: 2463293]

Nosyreva E, Szabla K, Autry AE, Ryazanov AG, Monteggia LM, Kavalali ET, 2013. Acute suppression of spontaneous neurotransmission drives synaptic potentiation. J. Neurosci. 33, 6990–7002. Available at: https://www.jneurosci.org/content/33/16/6990 [Accessed December 28, 2021]. [PubMed: 23595756]

Obradovic AL, Atluri N, Massara LD, Oklopcic A, Todorovic NS, Katta G, Osuru HP, Jevtovic-Todorovic V, 2018. Early exposure to ketamine impairs axonal pruning in developing mouse hippocampus. Mol. Neurobiol. 55, 164–172. [PubMed: 28840469]

O'Leary DDM, Stanfield BB, 1986. A transient pyramidal tract projection from the visual cortex in the hamster and its removal by selective collateral elimination. Dev. Brain Res. 27, 87–99.

Olney JW, Tenkova T, Dikranian K, Muglia LJ, Jermakowicz WJ, D' Sa C, Roth KA, 2002a. Ethanol-induced caspase-3 activation in the in vivo developing mouse brain. Neurobiol. Dis. 9, 205–219. Available at: http://www.sciencedirect.com/science/article/pii/S0969996101904759. [PubMed: 11895372]

Olney JW, Tenkova T, Dikranian K, Qin YQ, Labruyere J, Ikonomidou C, 2002b. Ethanol-induced apoptotic neurodegeneration in the developing C57BL/6 mouse brain. Dev. Brain Res. 133, 115–126. [PubMed: 11882342]

Paule MG, Li M, Allen RR, Liu F, Zou X, Hotchkiss C, Hanig JP, Patterson TA, Slikker W, Wang C, 2011. Ketamine anesthesia during the first week of life can cause long-lasting cognitive deficits in rhesus monkeys. Neurotoxicol. Teratol. 33, 220–230. [PubMed: 21241795]

PL H, CS R, F M, B T, 1989. N-methyl-D-aspartate receptors and ethanol: inhibition of calcium flux and cyclic GMP production. J. Neurochem. 52, 1937–1940. Available at: https://pubmed.ncbi.nlm.nih.gov/2542453/ [Accessed July 30, 2021]. [PubMed: 2542453]

Riccomagno MM, Kolodkin AL, 2015. Sculpting neural circuits by axon and dendrite pruning. Annu. Rev. Cell Dev. Biol. 31, 779–805. [PubMed: 26436703]

Sanchez V, Feinstein SD, Lunardi N, Joksovic PM, Boscolo A, Todorovic SM, Jevtovic-Todorovic V, 2011. General anesthesia causes long-term impairment of mitochondrial morphogenesis and synaptic transmission in developing rat brain. Anesthesiology 115, 992–1002. [PubMed: 21909020]

Schindelin J, Arganda-Carreras I, Frise E, Kaynig V, Longair M, Pietzsch T, Preibisch S, Rueden C, Saalfeld S, Schmid B, Tinevez JY, White DJ, Hartenstein V, Eliceiri K, Tomancak P, Cardona A, 2012. Fiji: an open-source platform for biological-image analysis. Nat. Methods 9 (7), 676–682. [PubMed: 22743772]

Singec I, Knoth R, Ditter M, Hagemeyer CE, Rosenbrock H, Frotscher M, Volk B, 2002. Synaptic vesicle protein synaptoporin is differently expressed by subpopulations of mouse hippocampal neurons. J. Comp. Neurol. 452 (2), 139–153. [PubMed: 12271488]

Sutton MA, Ito HT, Cressy P, Kempf C, Woo JC, Schuman EM, 2006. Miniature neurotransmission stabilizes synaptic function via tonic suppression of local dendritic protein synthesis. Cell 125, 785–799. Available at: http://www.cell.com/article/S0092867406005046/fulltext [Accessed March 27, 2022]. [PubMed: 16713568]

Szabadics J, Varga C, Brunner J, Chen K, Soltesz I, 2010. Granule cells in the CA3 area. J. Neurosci. 30, 8296–8307. Available at: https://www.jneurosci.org/content/30/24/8296 [Accessed December 29, 2021]. [PubMed: 20554881]

Tau GZ, Peterson BS, 2010. Normal development of brain circuits. Neuropsychopharmacology 35, 147–168. [PubMed: 19794405]

U.S. Food and Drug Administration, 2016. Drug Safety and Availability - FDA Drug Safety Communication: FDA review results in new warnings about using general anesthetics and sedation drugs in young children and pregnant women. Drug Saf Availab - FDA Drug Saf Commun FDA Rev results new Warn about using Gen Anesth Sedat drugs young Child pregnant women, pp. 1–11. Available at: https://www.fda.gov/Drugs/DrugSafety/ucm532356.htm [Accessed April 27, 2017].

U.S. Food and Drug Administration, 2018. FDA Drug Safety Communication: FDA review results in new warnings about using general anesthetics and sedation drugs in young children and pregnant women | FDA. Available at: https://www.fda.gov/drugs/drug-safety-and-availability/fda-drug-safety-communication-fda-review-results-new-warnings-about-using-general-anesthetics-and [Accessed October 3, 2021].

West JR, Hodges CA, Black AC, 1981. Prenatal exposure to ethanol alters the organization of hippocampal mossy fibers in rats. Science (80-) 211, 957–959.

Wilder RT, Flick RP, Sprung J, Katusic SK, Barbaresi WJ, Mickelson C, Gleich SJ, Schroeder DR, Weaver AL, Warner DO, 2009. Early exposure to anesthesia and learning disabilities in a population-based birth cohort. Anesthesiology 110, 796–804. [PubMed: 19293700]

Woodward TJ, Timic Stamenic T, Todorovic SM, 2019. Neonatal general anesthesia causes lasting alterations in excitatory and inhibitory synaptic transmission in the ventrobasal thalamus of adolescent female rats. Neurobiol. Dis. 127, 472–481. [PubMed: 30825640]

Yeckel MF, Berger TW, 1990. Feedforward excitation of the hippocampus by afferents from the entorhinal cortex: redefinition of the role of the trisynaptic pathway. Proc. Natl. Acad. Sci. U. S. A. 87, 5832–5836. [PubMed: 2377621]

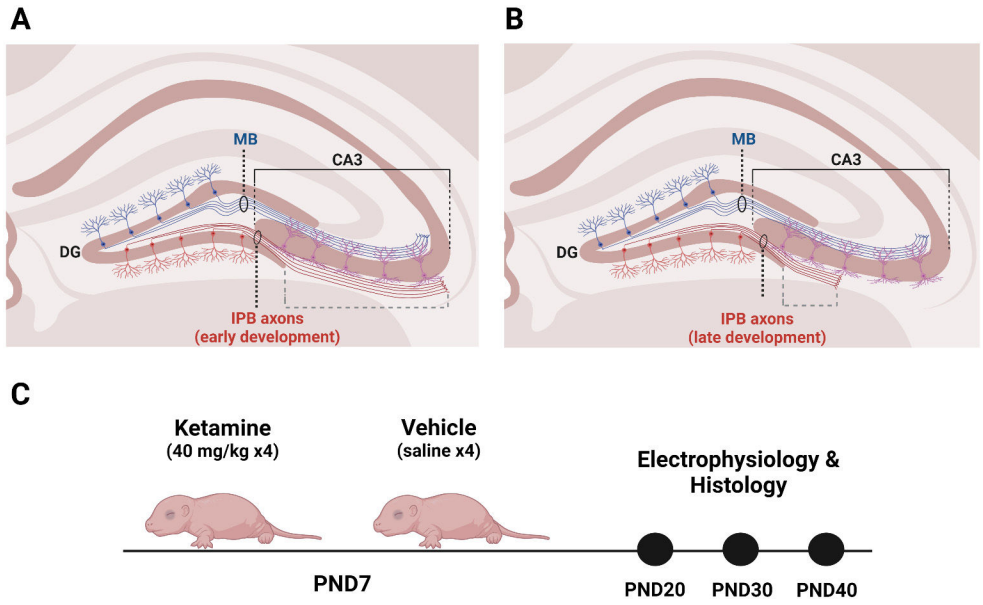

Fig. 1. Diagrams of stereotyped axonal pruning in the IPB of hippocampus and of experimental design.

A. In early rodent postnatal development, the IPB of the mossy fiber system arises from the axons of DG granule neurons. IPB fibers send axon collaterals that innervate the basal dendrites of neurons in CA3. **B.** Starting around PND20, the IPB undergoes stereotyped axonal pruning that continues until at least PND40. IPB axons distal to DG are pruned hundreds of microns towards source neurons in DG. When the pruning window closes, the IPB is short, innervating neurons more proximal to the DG. **C.** PND7 mice were injected with 40 mg/kg ketamine or vehicle then subjected to electrophysiological and histological analyses at three developmental stages coinciding with the window of IPB pruning early pruning (PND20), active pruning (PND30), and late pruning (PND40). Normalized IPB length was the measure of IPB pruning and calculated as the length of the IPB (dashed gray bracket in **A.** and **B.**) divided by the length of CA3 (solid black bracket in **A** and **B**). Created with BioRender.com.

DG, dentate gyrus; IPB, infrapyramidal bundle; MB, main bundle; PND, postnatal day.

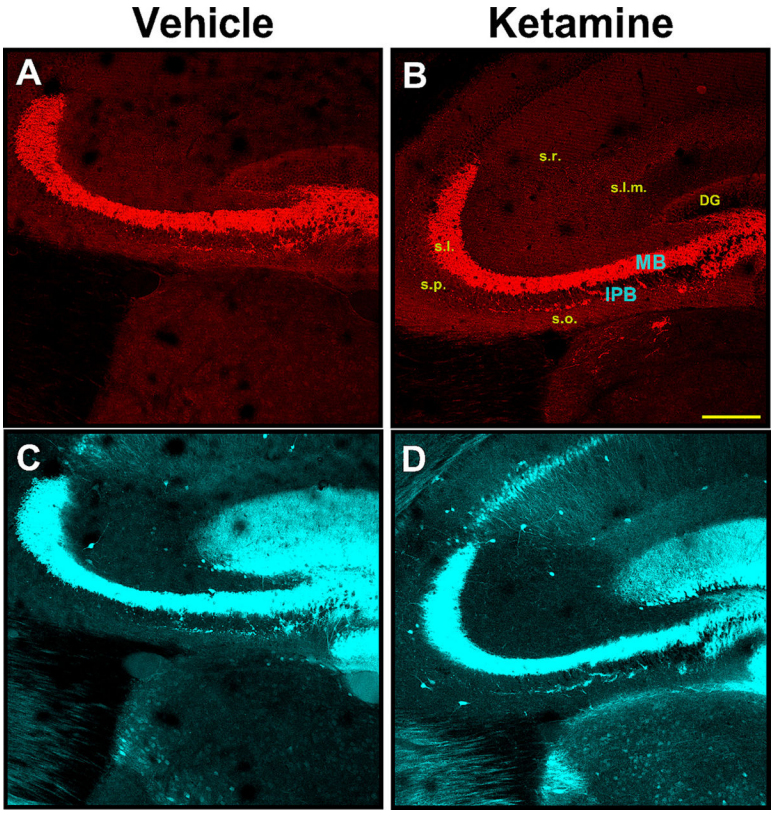

Fig. 2. Dual immunofluorescence staining indicates that synaptoporin more specifically labels mossy fiber system in mouse hippocampus compared to calbindin.

Dual immunofluorescence staining of synaptoporin (top panels – red) and calbindin (bottom panels – cyan) of representative PND40 animals following neonatal administration of vehicle **(A, C)** or ketamine **(B, D)**. Synaptoporin brightly stained mossy fibers of IPB and MB in stratum oriens and stratum lucidum, respectively; other areas were virtually devoid of the stain. Conversely, calbindin more broadly labeled hippocampal structures, extending into the stratum radiatum, stratum lacunosum-moleculare and dentate gyrus, in addition to areas that were also positive for synaptoporin. Virtually all synaptoporin-labeled structures showed almost complete colocalization of calbindin-stain; the reverse was not true. In all cases, IPB is readily observable as a bundle of fibers emanating from the tip of the inferior blade of the dentate gyrus, traversing the stratum oriens beneath the main bundle. Scale bar – 200 μm. (For interpretation of the references to colour in this figure legend, the reader is referred to the web version of this article.)

DG, dentate gyrus; IPB, infrapyramidal bundle; MB, main bundle; s.l.m., stratum lacunosum-moleculare; s.l., stratum lucidum; s.o., stratum oriens; s.p., stratum pyramidale; s.r. stratum radiatum.

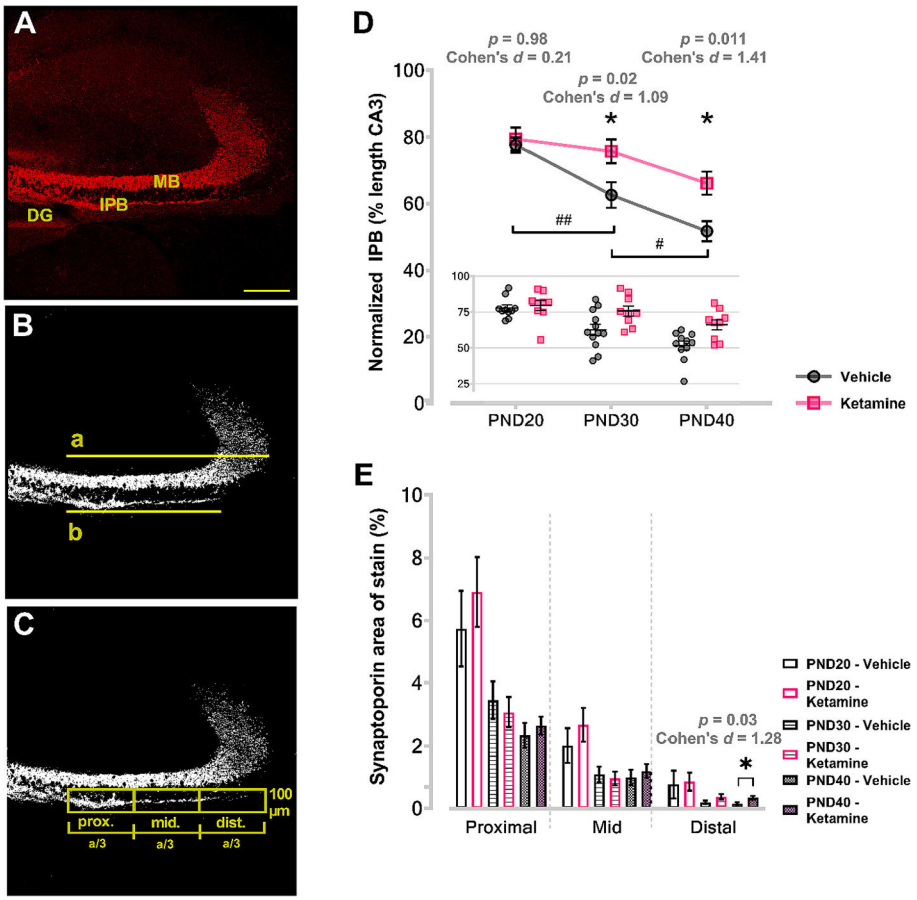

Fig. 3. Neonatal ketamine treatment impairs stereotyped axonal pruning in hippocampus.

Left panels show examples of measurements performed on a PND20 ketamine-treated animal. **Panel A** represents compressed 12 µM thickness stack of synaptoporin-stained coronal hippocampal section obtained with 10× objective and very high resolution (2048 × 2048). The compressed stack was thresholded and size-filtered for particles <0.5 µM diameter to eliminate the background noise (**B**). Measurements of CA3 MB (a) and IPB length (b) were then taken from the tip of the inferior blade of the DG, and normalized IPB ratio was obtained by dividing the two measurements (b/a). Next, the area that IPB traverses was divided into three rectangular areas (**C**) spanning exactly the distance measured with "a". The long axis of the rectangle equaled one-third of the MB length (a/3), whereas the short axis was constant and set at 100 µm for all images. The results were expressed as percent area positive for synaptoporin. Analysis of normalized IPB length (**D)** revealed that animals subjected to ketamine as neonates had significantly longer IPB at both PND30 and PND40 compared to vehicle counterparts (asterisks). Furthermore, IPB lengths between consecutive timepoints were significantly different in vehicle controls (pounds); in ketamine, they were not. Further analysis of IPB pruning revealed that percent area positive for synaptoporin immunolabeling was significantly higher in the most distal portions relative to DG in PND40 ketamine-treated animals compared to age and area-matched vehicle counterparts (**E**), indicating that distal sections of IPB were most affected by the process of stereotyped pruning. Scale bar – 200 µm.

DG, dentate gyrus; IPB, infrapyramidal bundle; MB, main bundle; PND, postnatal day.

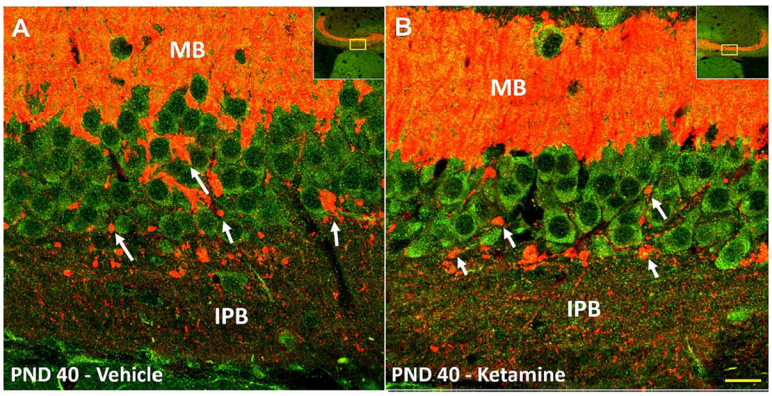

Fig. 4. Remaining IPB fibers likely make functional synapses with pyramidal layer neurons at PND40.

Immunofluorescence co-labeling of PSD-95 (green) and synaptoporin (red) in PND40 animal following neonatal vehicle (left panel) or ketamine (right panel), visualized with 60× objective. Multiple collaterals were observed emanating from the remaining IPB fibers as they migrate towards the MB. As these collaterals crossed the pyramidal layer, multiple large nodules (arrows) were detected in close proximity to PSD-95 positive pyramidal neurons, possibly *en passant* synapses, and also numerous small puncta around cell soma and basal dendrites. These histomorphological features of putative connections are indicative of functional synaptic connections between the presynaptic IPB terminals and CA3 pyramidal neurons. Insert is the 10× magnification image showing the location from which the 60× images were obtained. Scale bar – 20 μm. (For interpretation of the references to colour in this figure legend, the reader is referred to the web version of this article.)
IPB, infrapyramidal bundle; MB, main bundle; PND, postnatal day.

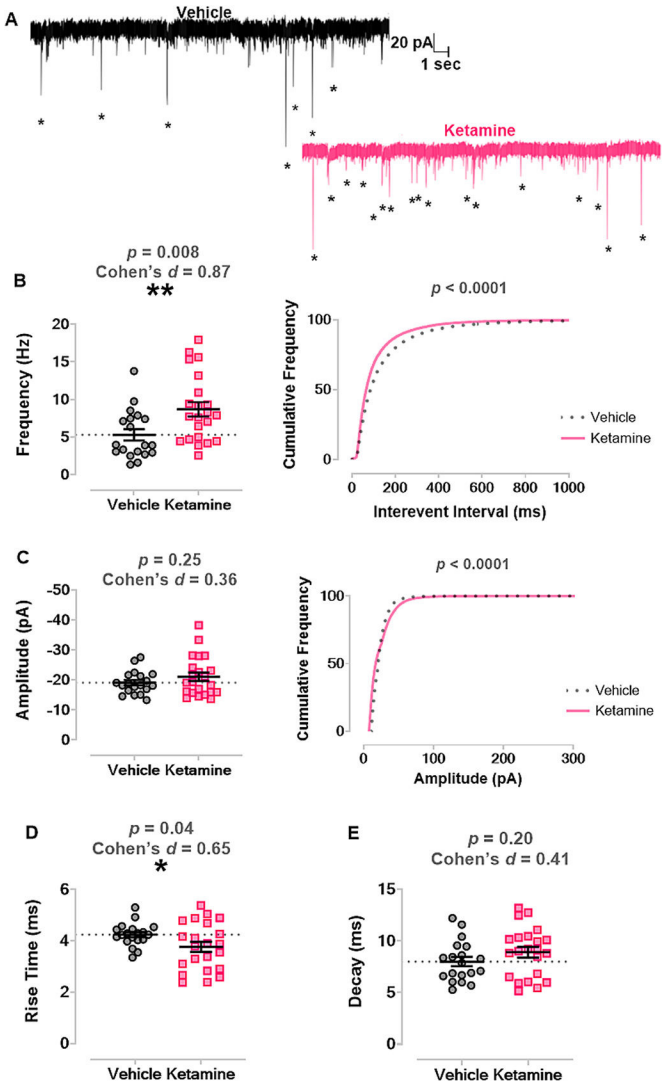

Fig. 5. Neonatal ketamine exposure increases excitatory synaptic transmission in CA3 at PND20.

A. Left panel shows representative trace of mEPSCs recorded from a juvenile mouse treated with vehicle as a neonate. Right panel displays representative trace of mEPSCs recorded from a mouse treated with ketamine as a neonate. Asterisks mark mEPSCs. **B.** Mice treated with ketamine as neonates (n = 9 mice, n = 19 neurons) had significantly increased frequency of mEPSCs in CA3 neurons compared to those treated with vehicle (n = 8 mice, n = 22 neurons) (**left panel**) and a significant leftward shift in the cumulative frequency of the interevent interval **(right panel**). **C.** There was no change in the average amplitudes of mEPSCs between groups (**left panel**), but there was a significant rightward shift in cumulative frequency of mEPSC amplitude (**right panel**). **D.** Neonatal ketamine also significantly shortened rise time of mEPSC events compared to vehicle. **E.** There was no change in decay of mEPSCs between groups.

mEPSC, miniature excitatory postsynaptic current; PND, postnatal day.

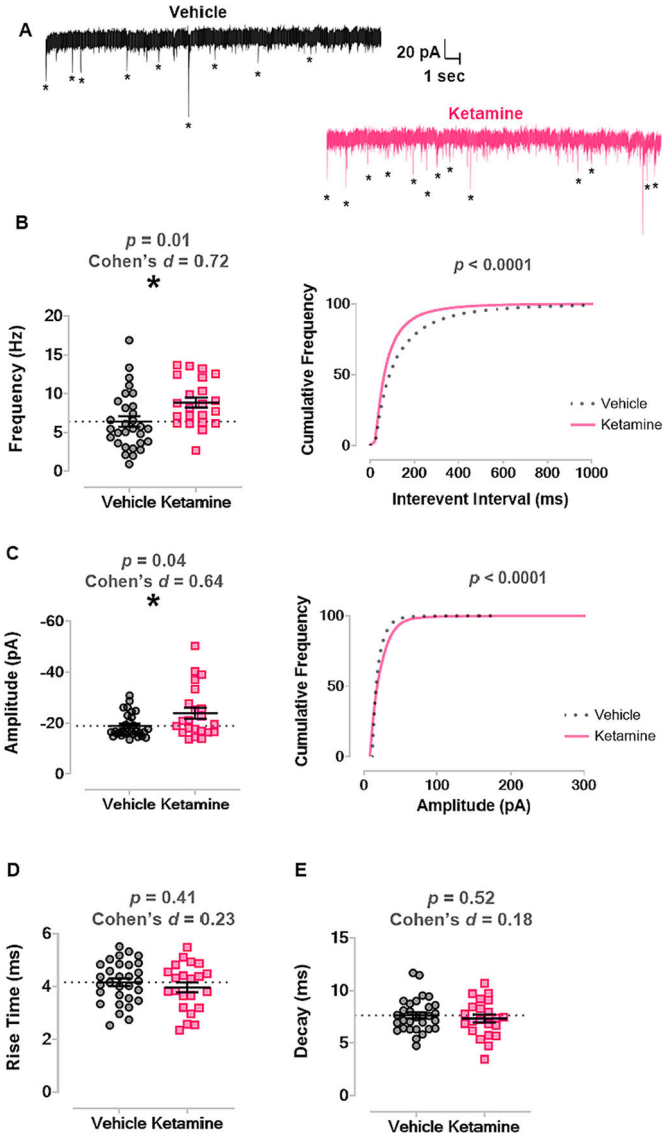

Fig. 6. Neonatal ketamine exposure significantly increased frequency and amplitudes of mEPSCs at later (PND30 and PND40) developmental stages.

A. Left panel shows representative trace of mEPSCs recorded from a vehicle treated mouse in later juvenile development. Right panel shows representative trace of mEPSCs from a mouse treated with ketamine as a neonate. Asterisks mark mEPSCs. **B.** Mice treated with ketamine as neonates ($n = 12$ mice, $n = 22$ neurons) had higher average frequency of mEPSCs compared to mice that received vehicle ($n = 11$ mice, $n = 30$ neurons) (**left panel**) and a leftward shift in mEPSC interevent interval (**right panel**). **C.** Neonatal ketamine caused an increase in average amplitude of mEPSCs compared to vehicle **(left panel)** and a rightward shift in cumulative frequency of mEPSC amplitude (**right panel**). **D.** There was no change in mEPSC rise time between groups. **E.** There was no change in mEPSC decay between groups.

mEPSC, miniature excitatory postsynaptic current; PND, postnatal day.